Structure of Electronically Reduced N-Donor Bidentate Ligands and Their Heteroleptic Four-Coordinate Zinc Complexes: A Survey of Density Functional Theory Results

Madanakrishna Katari, Duncan Carmichael, Denis Jacquemin, Gilles Frison

Structure of electronically reduced *N*-donor bidentate ligands and their heteroleptic four-coordinate zinc complexes: A survey of DFT results

Madanakrishna Katari,[a] Duncan Carmichael,[a] Denis Jacquemin,[b] Gilles Frison[a]*

[a] LCM, CNRS, Ecole polytechnique, IP Paris, F-91128 Palaiseau, France
[b] Univ. Nantes, CNRS, CEISAM (UMR 6230), 2 chemin de la Houssinière, 44322 Nantes, Cedex 03, France

Abstract

The role of Hartree-Fock exchange in describing the structural changes occurring upon reduction of bipyridine-based ligands and their complexes is investigated within the framework of density functional theory calculations. A set of 4 free ligands in their neutral and radical anionic forms, and 2 of their zinc complexes in their dicationic and monocationic radical forms, is used to compare a large panel of pure, conventional, and long-range corrected hybrid DFT functionals; coupled cluster single and double calculations are used alongside experimental results as benchmarks. Particular attention has been devoted to the magnitude of the change, upon reduction, of the Δ-parameter, which measures the difference between the C_{py}-C_{py} and the C-N bond lengths in bipyridine ligand and is known to experimentally correlate with the charge of the ligands. Our results indicate that the structural changes significantly depend on the amount of *exact* exchange included in the functional. A progressive evolution is observed for the free ligands, whereas two distinct sets of results are obtained for the complexes. Functionals with a small degree of HF exchange, *e.g.,* B3LYP, do not adequately describe geometric changes for the considered species and, quite surprisingly, the same holds for the CC2 method. The best agreement to experimental and CCSD values is obtained with functionals that include a significant but not excessive part of *exact* exchange, *e.g.*, CAM-B3LYP, M06-2X, and ωB97X-D. The calculated localisation of the added electron after reduction, which depends on the self-interaction error, is used to rationalize these outcomes. Static correlation is also shown to play a role in the accurate description of electronic structure.

Introduction

N-donor bidentate ligands (L) such as 2,2'-bipyridine (bpy) and 1,10-phenanthroline are able to form complexes with many transition metals. Their remarkable coordination behavior has been intensively exploited in organometallic and supramolecular chemistry,[1] as well as in main-group chemistry.[2,3] The photophysical and photochemical properties of these metal multipyridyl structures allow the design of complexes with interesting luminescent[4,5] or nonlinear optical properties.[6] These complexes can also undergo reversible redox processes, making them attractive building blocks in both artificial photosynthesis[7,8] and visible light photocatalysis.[9,10] Intense efforts have been made to better understand the structure and properties of these complexes, with both experimental and theoretical approaches being used to that end.[11-13]

Due to the non-innocent behavior of these ligands,[14] one of the essential questions relates to the electronic structure of their organometallic complexes and, more specifically, the repartition of the electronic density between the metal center and the ligands. This has been explored through a combination of various experimental methods such as Raman, UV-Vis, and magnetic susceptibility measurements or electron paramagnetic resonance (RPE) in condensed phase,[15-22] as well as with mass spectrometry and IR or UV-Vis photodissociation spectroscopies in the gas phase.[23-31] These approaches reveal a variety of electronic structures that depend on the nature of the complexes as well as their oxidation states. Examples range from reduced metal centers with neutral ligands such as $[Zn^{+}(L^{0})_{n}]^{+}$ (n = 1, 2 or 3) complexes[27,32] to complexes with reduced ligands such as $[Ru(bpy)_3]^{+}$ and $[Fe(bpy)_3]^{+}$. For the latter complexes, the most likely formulation is $[M^{2+}(bpy^{0})_2(bpy^{-1})]$,[17] which is also observed for the complex of Na^{+} coordinated by a reduced macrobicyclic tris(bipyridine) ligand.[33]

Other experimental data that can be used to investigate the electronic structure are provided by the geometric structure of the complexes. Indeed, based on the X-ray structure of neutral bpy^0,[34] monoanionic bpy^{-1} [35] and dianionic bpy^{-2},[35,36] it has been shown that the intramolecular CC and CN bond lengths of the bpy ligand vary as a function of the overall ligand charge because of changes in the bonding and antibonding interactions of the bpy^0 π^* orbital (lowest unoccupied molecular orbital, LUMO).[35] This structural signature, which has also been studied in other non-innocent ligands such as substituted bipyridine,[37-39] phenanthroline,[40] terpyridine,[38,39,41] pyridine-2,6-diimine[40] or quinones[42] is a good indicator of both the electronic population of the coordinated ligands and the electronic structure of the complexes.[43-47]

If high resolution X-ray crystallographic structures can be obtained, accurate bond lengths and the way in which they change upon varying the oxidation level can allow the redox state of the ligands in their coordination complexes to be determined unambiguously. Alternatively, a good correlation has been recently established between the ^{13}C NMR chemical shifts and the relevant bond lengths in non-innocent ligands at different levels of reduction.[48,49] Finally, and more frequently, geometrical structures are obtained through DFT calculations,[50] even if the DFT accuracy for bond length variations induced by electronic reduction remains to be established convincingly.

In addition to geometrical structure, DFT calculations can be used to model the electronic structure of the species through determining the occupied molecular orbitals and the spin density distribution.[51-54] In most cases, good agreement is found when comparing experimental and theoretical descriptions of the electronic structure. We nevertheless underline that discrepancies have been observed in some cases. For example, B3LYP calculations of $[Ru(bpy)_3]^{+}$ and $[Fe(bpy)_3]^{+}$

complexes lead to structures with three equivalent ligands, each carrying 1/3 of a spin. This corresponds to a single electron delocalized over the three ligands, $[M^{2+}(bpy^{-1/3})_3]$, which is in contradiction with the $[M^{2+}(bpy^{0})_2(bpy^{-1})]$ formulation based on experimental data.[17] Similarly, an electronic structure with spin density evenly distributed over the three bpy ligands is computed at the B3LYP level for $[Cr(bpy)_3]^{+1}$, whereas a more localized pattern $[Cr^{3+}(bpy^{0})(bpy^{-1})_2]$ can be inferred from experimental data.[37]

Globally, DFT methods are known to induce an overly disperse spin density after single-electron reduction or oxidation of closed-shell systems.[55] For example, it has been shown that the description of the ground state electronic structure of singly-reduced doubly protonated peptides is a problematic case for "conventional" DFT functionals, including local spin density approximation (LSDA) functionals, generalized gradient approximation (GGA) functionals, *meta*-GGA, and most of the global hybrid (GH) functionals. They also show excessively delocalized spin densities, comparable with those observed in charge-transfer excited states,[56-58] and this problem can be traced back to incorrect long-range behaviour resulting from the self-interaction error (SIE).[59] An accurate description of the ground state with DFT methods is obtained only if the functional includes full *exact* exchange (EXX, the amount of exchange within the Hartree-Fock formulation) at long-range interelectronic distance, even if this prerequisite is not always sufficient.[60] Other problematic cases have been described in the literature, e.g., manganese oxo[61] or iron nitrosyl complexes.[62] EXX has been shown to influence many computed properties, e.g. the spectoscopic properties of molecular systems,[63] spin-state ordering[64] or the ability of metal complexes to change spin state during a catalytic reaction.[65] To the best of our knowledge, there are no studies describing the effect of the chosen exchange-correlation functional on the electronic description of *N*-donor bidentate ligand radicals ($L^{\bullet-}$), or their $[M(L)_n]^{\bullet+}$ complexes obtained upon single-electron reduction of closed-shell systems. Such studies are particularly important with respect to the reliability of the B3LYP functional, which has been applied in countless related systems.[18-22,35-38,41,43-45,50-53,66-71]

A further point deserves attention with respect to the use of mono-reference DFT methods to study these compounds. It is known that static correlation can influence the electronic structure of transition metal complexes having non-innocent ligands,[48,52] notably in the case of iron complexes.[72] The multi-reference character arises from the electronic exchanges between the metal and the ligands. In this respect, zinc complexes constitute counter-examples where the multi-reference character is not pronounced,[52] unless the complex includes two radical ligands.[73] It should also be noted that whilst the analysis of the electronic structure of some of these complexes requires multi-reference calculations, the geometry optimization step is more usually performed at the DFT level. The choice of the functional used can have a significant impact on the optimized geometry, and therefore be crucial for the calculation of the electronic structure at the multi-reference level.

In the present work, a large selection of exchange-correlation DFT functionals is used to probe the structural changes upon reduction of *N*-donor bidentate ligands and their complexes and their representation of electronic structure in the resulting singly-reduced species. When possible, reference data determined experimentally[34,35] or at the coupled-cluster single and double (CCSD) level are used to benchmark the data obtained at the DFT levels. Two heteroleptic four-coordinate zinc complexes $\mathbf{I}^{n+}$ and $\mathbf{II}^{n+}$ (n = 1, 2) (Scheme 1) have been examined, as well as their free *N*-donor bidentate ligands (**1**-**3**), which include various chemical functionalities.[27,74-76] Those are expected to induce different chemical behavior[77] and in particular, contrasted spin distribution.[66,78]

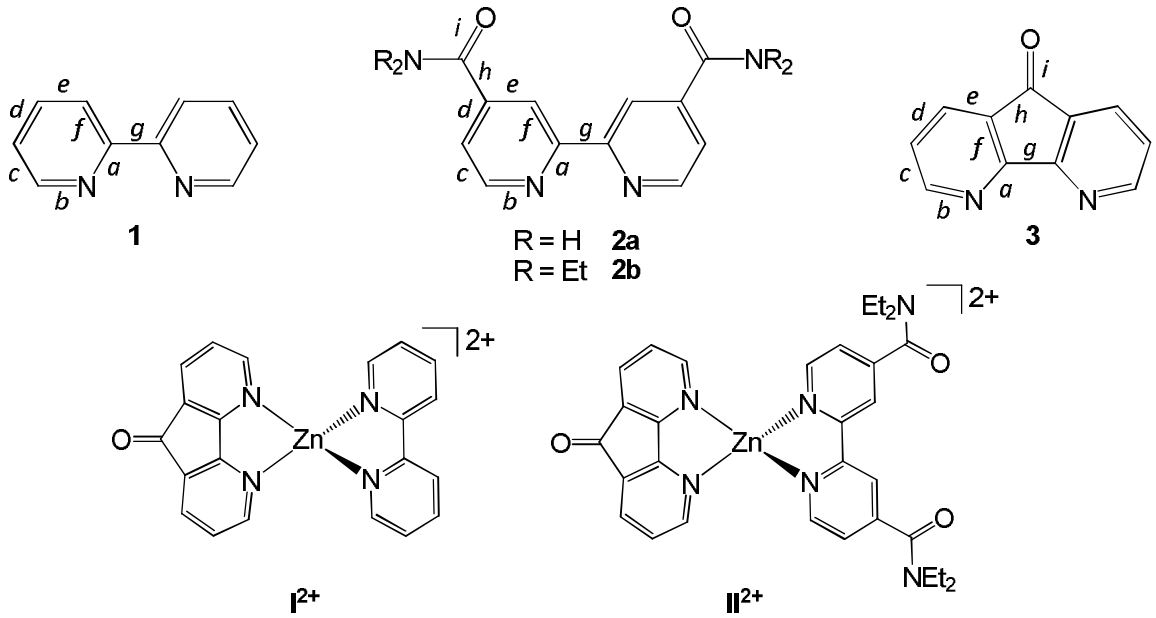

Scheme 1. Zn complexes **I**-**II** and the free *N*-donor bidentate ligands **1**-**3** studied in this work.

Computational methods

DFT calculations were carried out with the Gaussian09 package[79] and all structures were fully optimized without any symmetry constraints. Sixteen different exchange-correlation functionals, which cover different families from semi-local approaches to range-separated hybrid (RSH) functionals have been applied for these calculations. To simplify the presentation of the results, only the data for 11 functionals are presented in the text. Three different families of functionals are treated:

(i) The "B + LYP" family is based on the Becke exchange functional published in 1988[80] and the Lee-Yang-Parr correlation functional.[81] We have selected 4 functionals from this series: one generalized gradient approximation (GGA) functional BLYP which has 0% of EXX;[80] the hybrid-GGA B3LYP,[80-81] which includes 20% of EXX; and the RSHs CAM-B3LYP[82] and LC-BLYP,[83] which include 19/65 and 0/100% of EXX contribution at short/long-range, respectively. Their attenuation parameter amounts to 0.33 (CAM-B3LYP) and 0.47 (LC-BLYP).

(ii) The Minnesota suite developed in 2006 by Truhlar's group. It also includes 4 functionals: one meta-GGA functional M06-L (0% of EXX),[84] and three global hybrid-meta-GGA functionals M06,[85] M06-2X[85] and M06-HF[86] with 27, 54 and 100% of EXX respectively.

(iii) The "ωB97" RSHs family developed by the Head-Gordon group, which includes three RSHs functionals: ωB97X-D,[87] ωB97X[88] and ωB97.[88] These functionals present a 22.2/100, 15.77/100 and 0/100% of EXX contribution at short/long-range, respectively. Importantly, the transition from Kohn-Sham exchange to HF-like exchange is governed by the attenuation parameter ω whose value is 0.2, 0.3 and 0.4 a.u. for these three functionals, respectively. A larger ω value accelerates the transition from Kohn-Sham exchange to *exact* exchange. All three functionals show 100% EXX at long range, so that

ωB97X-D has a somewhat smaller EXX contribution and higher self-interaction errors than ωB97X and ωB97.[60a]

These 3 families provide a representative sample of the DFT functionals that are most often used in the literature. Within each family, the forms of DFT exchange and DFT correlation remain constant, allowing the effect of EXX on the properties under study to be estimated. Results for PBE (GGA functional, EXX=0%),[89] PBE0 (hybrid-GGA functional, EXX=25%),[90] TPSS (meta-GGA functional, EXX=0%),[91] TPSSh (hybrid-meta-GGA functional, EXX=10%)[92] and M11 (RSH functional, 42.8/100% of EXX at short/long range)[93] are in accordance to their EXX contribution compared to the results of the 11 functionals (see SI).

The def2-SVP atomic basis set, developed by Weigend and Ahlrichs,[94] has been used for geometry optimization at the DFT levels for all atoms. For each stationary point, we carried out a vibrational frequency calculation at the same level to characterize their nature as minima. Additional calculations have been performed with the 6-31G(d,p) and 6-31++G(d,p) basis sets for selected cases in order to evaluate the influence of diffuse functions upon the optimized geometries. These appear to have a significantly more limited impact than EXX on the bond length variations (see Figure S6 and Tables S4-S7).

In order to obtain reference structural data, the optimized geometry of ligands **1**, **2a** and **3** in their neutral and reduced forms, has been computed at the CCSD[95] and CC2[96] levels using Gaussian16,[97] Turbomole v7.1[98] and PSI4[99] software. CCSD and CC2 methods have recently been shown to give reasonable ground and excited state multiple bond lengths but with opposite errors relative to CCSDR(3): multiple bond lengths are found to be too short with CCSD, because of an overlocalized description of the ground and excited state geometries; the reverse is found for CC2.[100] In addition to the def2-SVP basis set, triple zeta basis sets 6-311G(d,p) and def2-TZVPP have been used with CCSD and CC2 methods, respectively, because it is known that the basis set size influences the geometries obtained with these post-HF methods.[101] Both "Frozen Core" (FC), with inner-shell electrons excluded from the correlation calculation, and "Full" approaches, in which all electrons are correlated, have been used with the CCSD method,[102] whereas all CC2 calculations have been done with the "Full" option. CC calculations took advantage of the point group symmetry when possible. These calculations, as well as additional calculations at the DFT levels, demonstrate that structural data for a given method are basically insensitive to the size of the basis set and/or to the correlation of the core electrons in CCSD calculations (*vide infra* and Tables S4-S6).

In order to ascertain that the wave functions of the open-shell species correspond to the minimum, their stability has been tested with the “stable” approach implemented in Gaussian with DFT. Calculations on all open-shell species (monoanionic ligands and monocationic complexes) used the spin-unrestricted formalism. In all DFT calculations, contamination by higher spin states was negligible to modest (the spin operator $\langle S^2 \rangle$ values are between 0.75 and 0.81). As might be expected, contamination by higher spin states was larger for coupled cluster calculations ($\langle S^2 \rangle$ up to ca. 1.50). The atomic spin density populations are obtained from the difference between α-spin and β-spin natural bond orbital (NBO) atomic charges[103] computed with the same level used for geometry optimization, whilst employing the larger def2-TZVPP basis set in the case of DFT calculations. They were performed with the NBO program implemented in Gaussian.

Static electron correlation diagnosis has been carried out for all compounds through a fractional occupation number weighted density (FOD) analysis performed with the ORCA 4.0 program.[104] FOD analyses have also been performed on CAM-B3LYP geometries for neutral and anionic ligands **1**-**3**, as well as dicationic and monocationic complexes **I** and **II**. The static electron correlation was quantified by the fractional orbital occupation (FO) as well as integration of the fractional orbital density ρ^{FOD} over all space (N_{FOD}). The procedure recommended[105] in the literature (TPSS method, def2-TZVP basis set, Fermi temperature at 5000 K) and successfully employed for open-shell compounds[106] was used to obtain these values.

Results and discussion

Static electron correlation diagnosis

Figure 1 shows the N_{FOD} values for ligands **1**-**3** and complexes **I**-**II**. Fractional orbital occupations are given in Table S1. Neutral ligands $\mathbf{1^0}$-$\mathbf{3^0}$ and dicationic complexes $\mathbf{I^{2+}}$ show negligible to small fractional orbital density due to incomplete occupation of the nitrogen and oxygen lone pairs (FO < 1.98) and small occupation of delocalized π^* orbitals (FO > 0.02). Surprisingly, a large N_{FOD} value (0.935) is obtained for $\mathbf{II^{2+}}$. In addition to intra-ligand electronic transfers of the type found in $\mathbf{1^0}$-$\mathbf{3^0}$ and $\mathbf{I^{2+}}$, significant transfers from **2b** ligand (π^* of the amide groups) into the π system of ligand **3** are also observed, whilst the metal center is not involved at all. With respect to radicals, all compounds have a large N_{FOD} (values between 0.668 and 1.624) that reflect two factors. Firstly, the effects observed prior to the addition of the single electron are retained for β orbitals, and this accounts for about 20% of the observed values. However, most of the fractional orbital density arises from the single electron, which is partially present in the delocalized π-orbital of the bipyridine moieties, but is also found in some of the virtual π orbitals. It is therefore clear that a good description of the electronic structure of these compounds requires the use of multi-reference methods, particularly in the case of radical species. The electronic structures obtained with the DFT functionals in the following should therefore be interpreted with caution. Given that the use of multi-reference methods is unlikely to be practical for optimizing the geometry of these compounds, an approximate mono-reference method such as a DFT functional needs to be used for this purpose if no experimental structure is available. In the rest of this work, we will therefore consider that static electron correlation does not strongly influence the differences between the close-shell and radical final structures of the geometry optimization process. This assumption is justified both by the results obtained for $\mathbf{1^0}$ and $\mathbf{1^{\bullet-}}$ for which a comparison with the experimental data is possible (vide infra), and by additional CAS-SCF multi-reference calculations showing only small effects on bond length variation upon reduction as compared to mono-reference calculations (see Table S2 in the SI).

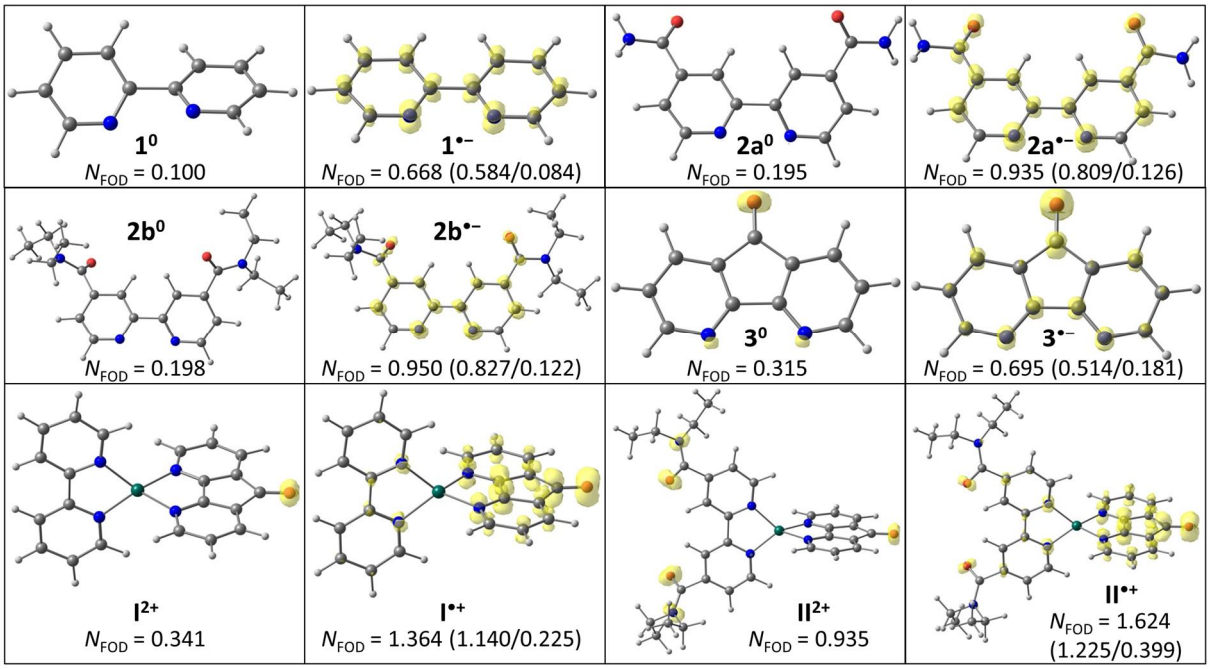

Figure 1. Fractional orbital density ρ^{FOD} isosurfaces (in yellow) at 0.005 e.Bohr^{-3} as calculated at the TPSS/def2-TZVP (T = 5000 K) for neutral and radical ligands **1**-**3** and dicationic and monocationic complexes **I**-**II**. N_{FOD} values in parentheses correspond to the N_{FOD} for α/β spin density. see Figure S14 for isosurfaces at 0.002 e.Bohr^{-3}.

Single reduction of the free ligands

We started our study of bond length variations that occur upon single electron reduction by looking at the free neutral ligands **1**^{0}-**3**^{0} and their mono-electronic reduced forms **1**$^{\bullet-}$-**3**$^{\bullet-}$, respectively. The geometries of these neutral and anionic species were optimized in their *cisoid* forms so as to retain a consistent ligand conformation throughout the study, but we have demonstrated in the case of **1**^{0} that *cis-trans* isomerization provides similar results and conclusions (see Table S3). Methods employed for these geometry optimizations include the eleven functionals selected in this work, as well as both the CC2 and CCSD levels, except for the largest ligand **2b**. As expected,[107] **1**^{0}, **2a**^{0} and **2b**^{0} present a twisted structure around the central CC bond separating the 6-membered rings, whereas their anionic forms, as well as **3**^{0} and **3**$^{\bullet-}$, show almost planar geometries except for the C(O)NR$_2$ substituents of **2a**$^{\bullet-}$ and **2b**$^{\bullet-}$.

The single reduction of neutral *N*-donor bidentate ligands **1**-**3** induces changes in the CC, CN and CO bond lengths. All calculations indicate that the incoming electron occupies a SOMO orbital that strongly resembles the LUMO of the neutral system **1**^{0}-**3**^{0} (Figure 2).

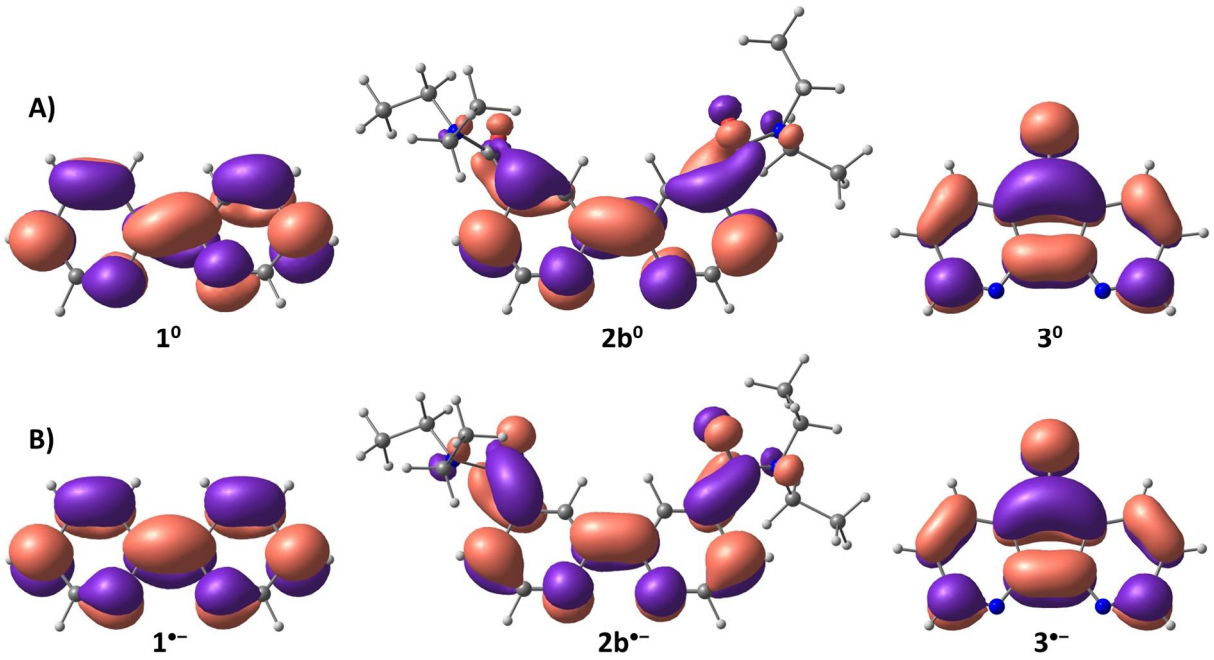

Figure 2. Lowest unoccupied molecular orbital (LUMO) of **1**-**3** (A), and the singly occupied molecular orbital (SOMO) in their respective monoanionic reduced form (B) computed at the BLYP level. Results for **2a** are similar to those obtained for **2b**. Isosurface value: 0.03 a.u.

Consequently, the CC, CN, and CO bond length variations upon reduction reflect the bonding or antibonding nature of these bonds in the LUMO of the neutral system.[35] Furthermore, for all ligands, a highly similar LUMO is obtained using the various functionals (Figure S1). Despite the good qualitative agreement between the bond length variations obtained using the functionals under evaluation, quantitative differences can nevertheless be observed as a function of the method employed. Examination of the results for each individual bond (Figures S2-S5) shows that some bond length variations are not affected by the level of calculation, while others are. For example, the *a* CN bond length of **1** (see Scheme 1 for numbering) increases upon reduction by 0.040 to 0.043 Å for all DFT functionals. In contrast, electronic reduction of **2a** induces almost equal changes in *b* CN and *f* CC bond lengths (+0.002 Å) at the BLYP level whereas M06-HF yields either opposite (-0.009 Å for *b*) or larger (+0.033 Å for *f*) variations. This obviously hints at an interplay between the amount of EXX and the computed bond length variations.

In order to describe these data more concisely, we analyzed two structural parameters: the Root Mean Squared Deviation (RMSD) of the bond length variations relative to reference values (Table 1) and the variation of Δ-parameter ($\Delta = g - a = [d(C_{py}\text{-}C_{py}) - d(C\text{-}N)]$), noted $\Delta\Delta$, used recently as a tool to characterize the electronic charge of the ligands (Figure 3).[38,40] Two forms of reference have been used. First, we use experimental X-ray crystal structure available in the literature for $\mathbf{1}^{\mathbf{0}}$ [34] and $\mathbf{1}^{\bullet-}$.[35] For the second, we optimize the geometry of $\mathbf{1}^{\mathbf{0}}$ and $\mathbf{1}^{\bullet-}$ and, when possible, of $\mathbf{2a}^{\mathbf{0}}$, $\mathbf{2a}^{\bullet-}$, $\mathbf{3}^{\mathbf{0}}$ and $\mathbf{3}^{\bullet-}$, at the CCSD and CC2 levels using different atomic basis sets, and use the CC results to evaluate the quality of the DFT predictions.

Table 1. Root Mean Squared Deviation (RMSD, in 10^{-2} Å) of the bond length variations relative to experimental or CCSD values.[a]

Method	Basis set	RMSD **1**/Exp[c]	RMSD **1**/CCSD[d]	RMSD **1-3**/CCSD[e]
BLYP	def2-SVP	0.747	0.703	1.078
B3LYP	def2-SVP	0.623	0.496	0.768
CAM-B3LYP	def2-SVP	0.563	0.243	0.296
LC-BLYP	def2-SVP	0.648	0.246	0.390
M06-L	def2-SVP	0.797	0.800	1.030
M06	def2-SVP	0.657	0.547	0.689
M06-2X	def2-SVP	0.577	0.312	0.328
M06-HF	def2-SVP	0.708	0.315	0.517
ωB97X-D	def2-SVP	0.550	0.239	0.294
ωB97X	def2-SVP	0.578	0.188	0.303
ωB97	def2-SVP	0.607	0.205	0.361
CCSD(FC)	6-311G(d,p)	0.469	0	0
CCSD(Full)	6-311G(d,p)	0.465	0.023	0.058[f]
CCSD(Full)	def2-SVP	0.528	0.166	0.175
CC2	def2-SVP	1.045	1.048	1.426[g]
CC2	def2-TZVPP	1.020	1.095	1.735[g]
Exp[b]		0	0.469	-

[a] See Scheme 1 for the considered bond lengths noted *a-i*. [b] Experimental values from refs 35 (K_4(2,2'-bpy)$_4$(ethylenediamine)) and 34 (2,2'-bpy). [c] RMSD values for the bond length variations in **1**, i.e., magnitude of the change between the bond lengths in neutral $\mathbf{1^0}$ and in radical anionic $\mathbf{1^{\bullet-}}$ species, relative to experimental values. [d] RMSD for the bond length variations in **1** relative to CCSD(FC)/6-311G(d,p) values. [e] RMSD for the bond length variations in **1**, **2a**, and **3** relative to CCSD(FC)/6-311G(d,p) values. [f] RMSD only for **1** and **3**, as $\mathbf{2a^{\bullet-}}$ could not been obtained at the CCSD(Full)/6-311G(d,p) level. [g] RMSD only for **1** and **2a**, as $\mathbf{3^{\bullet-}}$ could not been obtained at the CC2 level.

Results in Table 1 show low RMSD values (about 10^{-2} Å). Rather than referring to the bond lengths themselves, these are given for bond length variations which, even though they are small, are normally used to characterize the electronic charge of the ligands. Thus, among the *a-g* bonds of **1**, the largest variation upon reduction observed by X-ray is 6.1 10^{-2} Å and the RMSD between the neutral and reduced forms is 3.283 10^{-2} Å. Values of similar magnitude are obtained for all ligands at the DFT level. For example at the B3LYP level, RMSD values are 3.063, 1.993, 2.026 and 2.577 10^{-2} Å respectively for **1**, **2a**, **2b** and **3** between the neutral and reduced forms. On average, this indicates that, for some methods, the error in bond length variations can be almost the same order of magnitude as the variations themselves.

More specifically, results in Table 1 concerning bond length variations for **1** indicate that CCSD/6-311G(d,p) provides the most accurate computed results compared to experiment. This justifies its use as a reference, even if CCSD is known to provide multiple bond lengths in small conjugated organic molecules that are slightly too short.[100a] The results obtained with the Frozen Core option are used as a reference because they are very similar to those obtained when including all orbitals in the post-HF calculation and are less computationally demanding, which made it possible to perform them on all the organic compounds studied.

As stated above, the amount of *exact* exchange in the functional has a noticeable influence on the computed bond length variations. Relative to the experimental values for **1**, the most accurate

functionals in each family for evaluating changes in bond lengths upon reduction appear to be CAM-B3LYP, M06-2X, and ωB97X-D. This result is confirmed by the study of compounds **1**-**3**, for which comparison can only be made with CCSD data. Indeed, relative to CCSD, those GGA functionals and hybrid functionals having 20-27% of EXX give RMSD values that are roughly three and two times larger respectively than RSH functionals and hybrid functionals that have more than 50% of EXX. In contrast, functionals with the largest amount of EXX (LC-BLYP, M06-HF, and ωB97) give slightly less accurate results compared to those with a more balanced repartition between Kohn-Sham and HF-like exchanges (CAM-B3LYP, M06-2X, ωB97X-D, and ωB97X). Surprisingly, the largest deviation relative to both experimental and CCSD values is observed for CC2, which appears to be inadequate to reproduce the bond changes upon reduction.

A more in-depth analysis (see Table S8) of the calculated bond lengths reveals the origin of the above observed deviation. For $\mathbf{1}^{0}$ and $\mathbf{1}^{\bullet-}$, low RMSD values relative to experiment indicate that all levels of calculation provide accurate geometries with, however, a slightly greater deviation in the case of anions. The calculated bond lengths for $\mathbf{1}^{0}$-$\mathbf{3}^{0}$ and $\mathbf{1}^{\bullet-}$-$\mathbf{3}^{\bullet-}$ also broadly show a good agreement for all levels of calculation compared to CCSD values. More specifically, the deviation relative to CCSD is similar for both neutral and anionic compounds in most cases, except for BLYP, B3LYP, M06, M06-L, and CC2 where larger discrepancies are obtained for the anions. This indicates that these methods appear to be less adequate to accurately reproduce the structure of the radical anions than the neutral species.

Similarly, the variation of the Δ-parameter is sensitive to the level of calculation (Figures 3 and S6). In all cases, the lengthening of the CN bond *a* and the shortening of the CC bond *g* that accompany reduction means that value of the Δ-parameter decreases from the neutral to the anionic structure, implying negative values for ΔΔ. Once again, this structural value is highly sensitive to the amount of *exact* exchange in the DFT calculations, ranging for example from -0.043 Å with BLYP to -0.101 Å with M06-HF for **2a**. Comparisons with the experimental[34,35] and calculated CCSD reference values confirm that the best agreement is obtained with CAM-B3LYP, M06-2X, and ωB97X-D, i.e., functionals involving a very large amount of EXX (compared to the functional usually applied to model metal complexes) but not the huge contribution found in LC-BLYP, M06-HF or ωB97.

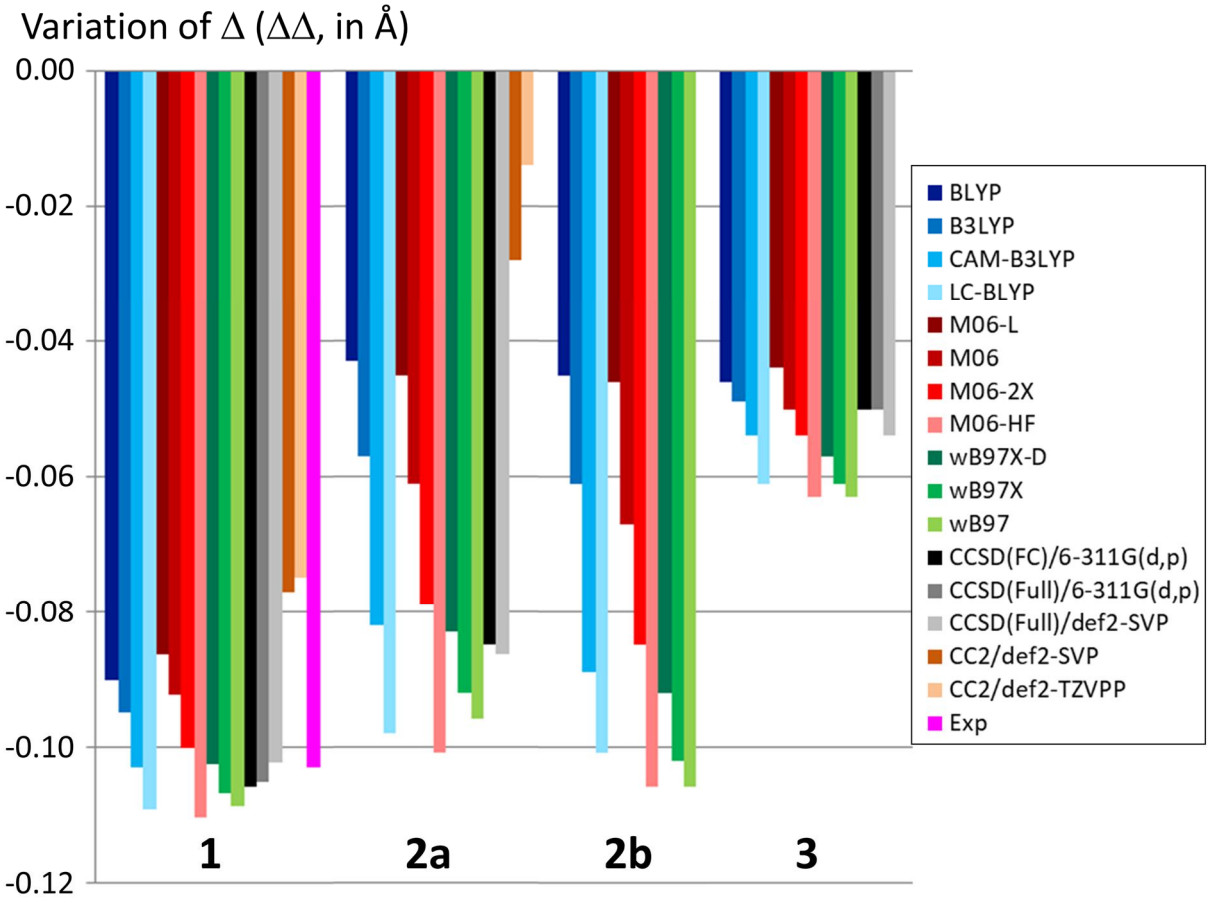

Figure 3. Variation of $\Delta = g - a$ ($\Delta\Delta$, in Å) for ligand **1**-**3** upon single-reduction estimated at various level of calculations. DFT calculations with the def2-SVP basis set; Experimental values from refs 35 (K_4(2,2'-bpy)$_4$(ethylenediamine)) and 34 (2,2'-bpy).

In order to get further insights, we now turn our attention to the electronic structure of the neutral and anionic ligands. As noted above, the level of calculation does not influence the qualitative description of the electronic structure of the neutral closed-shell ligands, as illustrated by the great similarities of the LUMO obtained with various functionals (Figure S1). On the other hand, weak differences in the electronic structure of the singly-reduced systems are observed depending on the functional used (Figures 4 and S7-S9). Increasing the EXX ratio, e.g., going from BLYP to LC-BLYP in Figure 4, induces a small decrease of the single electron delocalization over the whole π-system of **1**$^{\bullet-}$ Furthermore, since the calculations are performed with unrestricted wavefunctions, we observe that an increasing amount of EXX leads to larger spin-polarization, i.e., larger amount of atomic α and β spin densities on the carbon and nitrogen atoms of the six-membered ring, as has already been observed for radical cations of photosynthetic pigment models.[108] Comparison with the CCSD reference values (Figures S7-S9) indicates that the most trustworthy results are obtained for CAM-B3LYP and ωB97X-D, which is consistent with the above analysis. In a more marked way, the delocalization of the spin-density over the amide moiety in **2a**$^{\bullet-}$ and **2b**$^{\bullet-}$ is diminished when increasing the amount of EXX.

DFT functionals which include a small contribution from EXX are known to yield spin densities that suffer significantly from the self-interaction error.[59,108] This incorrect behavior also applies to the

electronic structure of anionic radical ligands $\mathbf{1}^{\bullet-}$-$\mathbf{3}^{\bullet-}$. Concomitantly the geometry change upon reduction is related to the localization of the added electron. So it implies that the SIE plays a noticeable role in the ability of the functional to describe structural properties such as the Δ parameter.

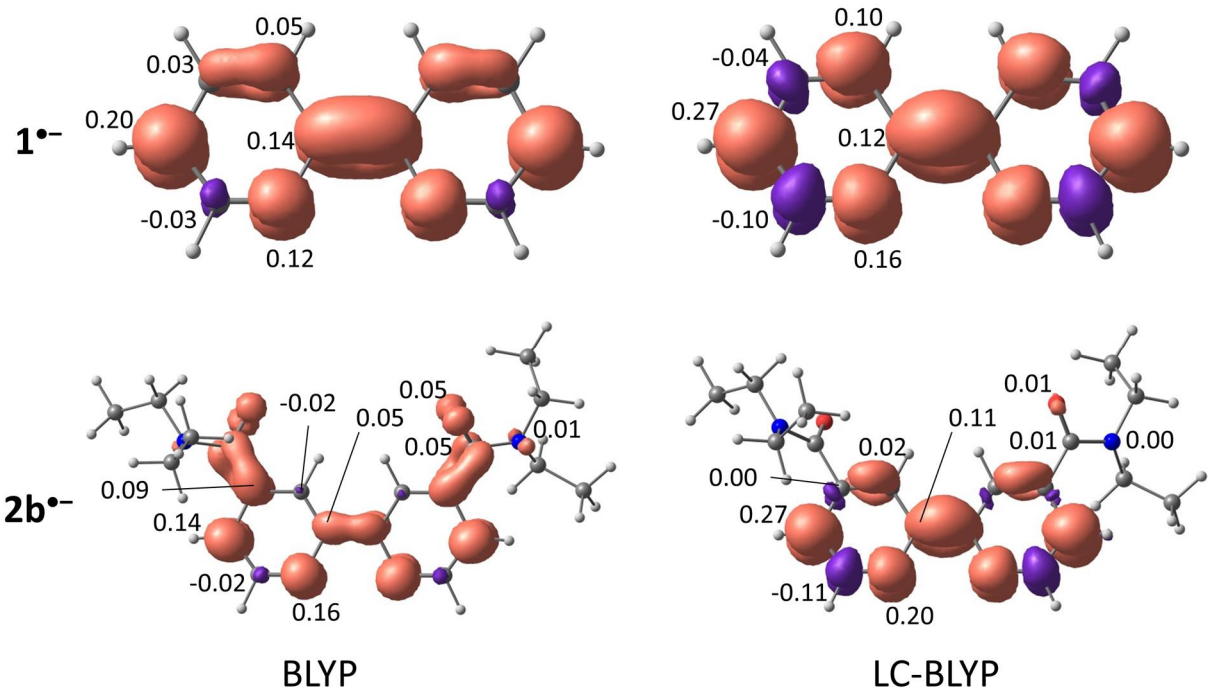

Figure 4. Spin density (isosurface value: 0.0025 a.u.) and NBO atomic spin density population (α-β) for $\mathbf{1}^{\bullet-}$ and $\mathbf{2b}^{\bullet-}$ computed with the BLYP and LC-BLYP functionals.

Single reduction of the zinc complexes

We now turn our attention to the single reduction of the two heteroleptic four-coordinate zinc complexes $[Zn(\mathbf{1})(\mathbf{3})]^{2+}$ and $[Zn(\mathbf{2b})(\mathbf{3})]^{2+}$, named respectively $\mathbf{I}^{2+}$ and $\mathbf{II}^{2+}$ (Scheme 1).

As for the ligands, we first examine for complexes $\mathbf{I}^{2+}$ and $\mathbf{II}^{2+}$ the bond length variations upon reduction with the eleven DFT functionals. The more significant data obtained for **I** and **II** are shown in Figure 5 (See Figures S10 and S11 for complete results). As observed for the free ligands, the bond length variations are functional-dependent and the amount of EXX has a marked impact on the predicted structural changes upon reduction.

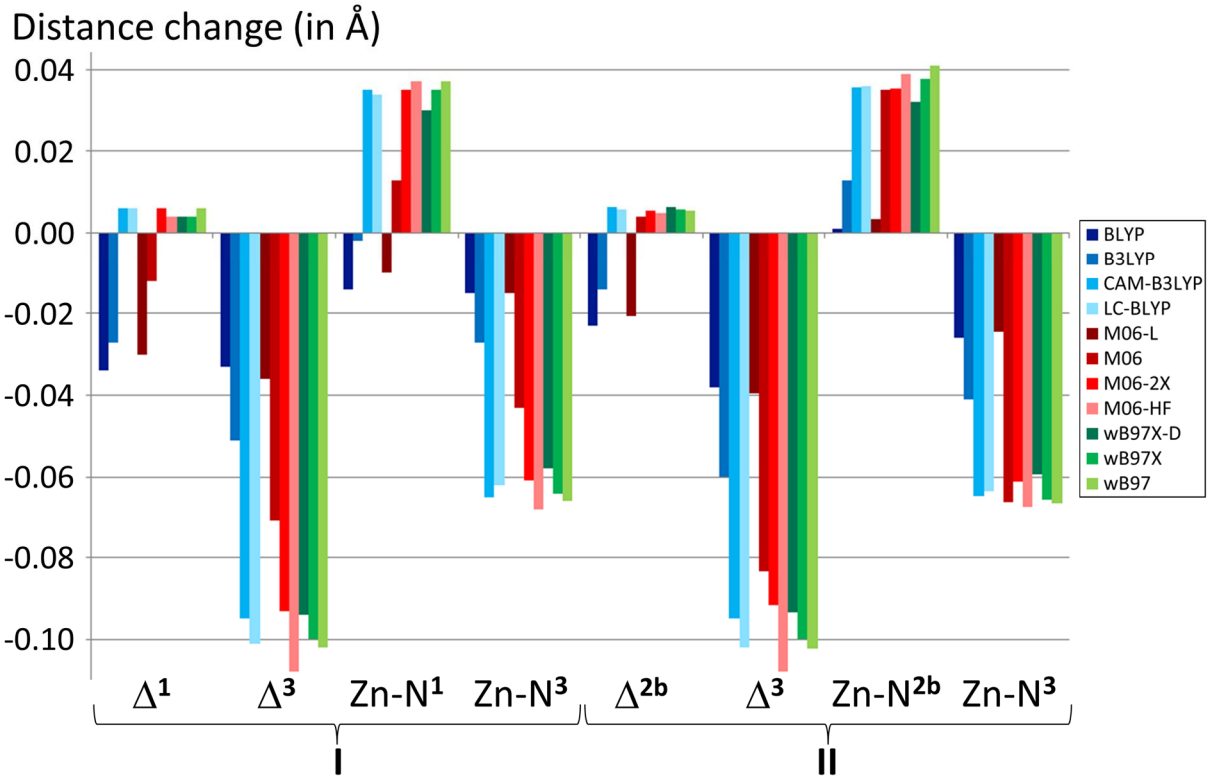

Figure 5. Δ parameter and Zn-N bond length variations between dicationic and singly-reduced radical monocationic states for complexes **I** and **II**. See Scheme 1 for the definition of the bonds.

In most cases, the differences between functionals are only quantitative, with bond length variations that are more or less marked, even if the differences can be significantly larger than for the free ligands. For example, upon reduction, the Δ-parameter of ligand **3** in **I**/**II** decreases by -0.033/-0.038 and -0.101/-0.102 Å at the BLYP and LC-BLYP levels, respectively, whereas it is shortened by -0.046 and -0.061 Å in the free ligand **3** (Figure 3). One can also note specific phenomena for these complexes. First, bond length variations of opposite signs are obtained when comparing conventional and long-range corrected hybrid functionals. In particular, the Zn-N distance between ligand **1** and the metal cation in **I** shortens upon reduction at the BLYP, B3LYP, and M06-L levels but lengthens with the other functionals. Similar observations are also obtained in some cases for the Δ-parameter. Secondly, in contrast to the free ligand cases, the bond lengths remain almost unchanged in ligands **1** (complex **I**) and **2b** (complex **II**) for all methods but BLYP, B3LYP, M06-L, and M06, i.e., the functionals presenting the smallest EXX ratio. From this analysis, it appears that the functional behavior allows the separation of the functionals into 2 distinct groups within which the structural changes are very similar. B3LYP, B3LYP and M06-L belong to the first group and CAM-B3LYP, LC-BLYP, M06-2X, M06-HF, ωB97X-D, ωB97X and ωB97 are in the second one, whereas M06 seems to be the only functional with a somewhat mixed behavior.

An explanation of these significant geometrical differences can be deduced from the examination of the SOMO (or the spin density) after reduction (Figures 6 and S12-S13). Indeed, at the BLYP, B3LYP, M06-L and, to a lesser extent M06, levels, the added electron in the optimized geometry of $\mathbf{I}^{\bullet+}$ and $\mathbf{II}^{\bullet+}$ is delocalized over both ligands, whereas, for all other methods, the added electron is fully located on the ligand **3**.

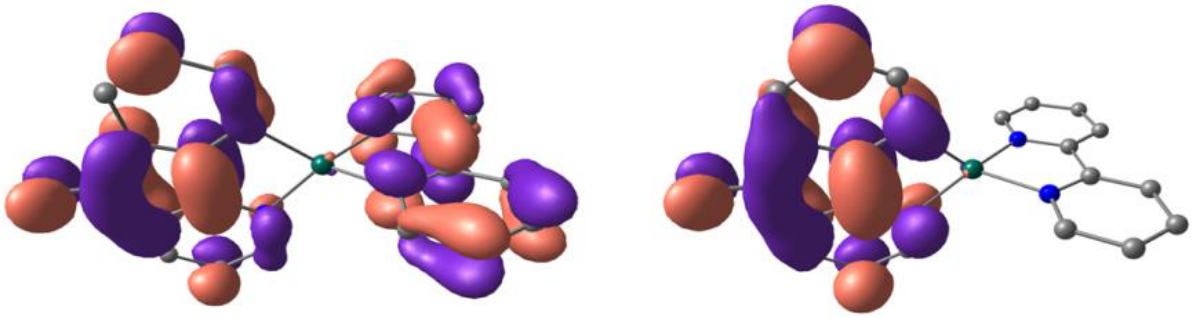

Figure 6. SOMO of $\mathbf{I}^{\bullet+}$ computed at the B3LYP (left) and LC-BLYP (right) level. Isosurface value: 0.03 a.u

Table 2. NBO spin density population of the ligands of $\mathbf{I}^{\bullet+}$ and $\mathbf{II}^{\bullet+}$ after vertical and adiabatic reduction of $\mathbf{I}^{2+}$ and $\mathbf{II}^{2+}$. Calculations at the DFT/def2-TZVPP//DFT/def2-SVP level.[a]

	I				**II**			
	Vertical reduction		Adiabatic reduction		Vertical reduction		Adiabatic reduction	
	1	**3**	**1**	**3**	**2b**	**3**	**2b**	**3**
BLYP	0.44	0.56	0.42	0.58	0.39	0.60	0.36	0.64
B3LYP	0.41	0.58	0.32	0.68	0.36	0.64	0.22	0.78
CAM-B3LYP	0.00	1.00	0.00	1.00	0.00	1.00	0.00	1.00
LC-BLYP	0.00	1.00	0.00	1.00	0.00	1.00	0.00	1.00
M06-L	0.43	0.57	0.40	0.60	0.39	0.60	0.35	0.65
M06	0.40	0.59	0.18	0.81	0.35	0.65	0.02	0.97
M06-2X	0.05	0.94	0.00	1.00	0.00	1.00	0.00	1.00
M06-HF	0.00	1.00	0.00	0.98	0.00	1.00	0.00	0.98
ωB97	0.00	1.00	0.00	1.00	0.00	1.00	0.00	1.00
ωB97X	0.00	1.00	0.00	1.00	0.00	1.00	0.00	1.00
ωB97X-D	0.00	1.00	0.00	1.00	0.00	1.00	0.00	1.00

[a] Spin density at the zinc metal center is in all cases smaller than 0.01 electron.

Closer examination of the spin density distribution on $\mathbf{I}^{\bullet+}$ and $\mathbf{II}^{\bullet+}$ delivers interesting trends (Table 2). Both after vertical and adiabatic reduction, the added electron is entirely located on ligand **3** only with the CAM-B3LYP, LC-BLYP, M06-HF, ωB97X-D, ωB97X, and ωB97 functionals. M06-2X shows almost the same behavior, except for the vertical reduction of $\mathbf{I}^{2+}$ for which a small electron delocalization on ligand **1** is also obtained. This very low electronic delocalization obtained for the optimized structure of the dicationic complex does, however, have only a trifling impact on the geometrical and electronic structure after optimization of the reduced complex geometry. BLYP, B3LYP, M06-L, and M06 show spin density on both ligands in all cases. However, delocalization is less marked for M06, which explains the intermediate structural results obtained with this functional. It is noticeable that the amount of spin density on **1** (in $\mathbf{I}^{\bullet+}$) and in **2b** (in $\mathbf{II}^{\bullet+}$) is directly related to EXX ratio included in the functional. Indeed, B3LYP and M06 show lower spin density on **1** and **2b** compared respectively to BLYP and M06-L. We also note that the delocalization over the two ligands slightly decreases upon geometry optimization.

The data of Table 2 also indicate that ligand **3** systematically takes the majority or the totality of the spin density. This agrees with its higher electron affinity compared to **1** and **2b** that stems from the strong conjugation between the CO moiety and the bipyridine frameworks.

These differences in the spin density distribution explain the differences in bond length variations. The $[Zn^{2+}(\mathbf{1}^{0})(\mathbf{3}^{\bullet-})]$ electronic structure of $\mathbf{I}^{\bullet+}$ computed with the long-range corrected functionals explains that: (*i*) the intramolecular bond lengths in **1** remain almost unchanged upon reduction; (*ii*) the Zn-N bond lengths between Zn and **3** decrease due to Coulombic effects, inducing lower Lewis acidity of the metal center and thus a longer Zn-N bond length between Zn and **1**. In contrast, the $[Zn^{2+}(\mathbf{1}^{-1/2})(\mathbf{3}^{-1/2})]$ electronic structure given by conventional DFT, *e.g.*, B3LYP, leads to molecular geometry in which both ligands are more tightly bound to the metal center.

Conclusions

It is now well established that oxidation and reduction processes induce characteristic intramolecular bond length variations in bipyridine-type non-innocent ligands coordinated to a metal center. Consequently, these geometrical changes have become markers of the electronic charge carried by the ligands, and consequently of the electronic structure of the related metal complexes. In this work, we have explored the ability of a large panel of DFT functionals, ranging from GGA to RSHs, to determine these bond length variations in four *N*-donor bidentate ligands as well as in two of their tetracoordinated zinc complexes. Depending on the functional selected for the calculations, negligible to significant errors in bond length variations have been obtained upon reduction. The differences stem from the different electronic structures provided by the various calculation methods, showing either a localized or a delocalized behavior of the added electron. These results can be explained by the amount of *exact* exchange included in the selected DFT functionals.

For the free ligands, the structural changes due to the spin density distribution in the π system follow a gradual change that is related to the amount of *exact* exchange. Comparison with experiment and CCSD values indicates that the most accurate results are obtained for a significant but not excessive correction of the self-interaction error, as given by the CAM-B3LYP, M06-2X, and ωB97X-D functionals. For $[Zn(L)(L')]^{\bullet+}$-type structures, a delocalized $[Zn^{2+}(L^{-1/2})(L'^{-1/2})]$ electronic structure is computed with BLYP, B3LYP, M06-L, and M06 functionals whereas a single-ligand localized $[Zn^{2+}(L^{\bullet-})(L'^{0})]$ electronic structure is obtained with CAM-B3LYP, LC-BLYP, M06-2X, M06-HF, ωB97X-D, ωB97X, and ωB97. Results for the free ligands are in agreement with previous studies and strongly hint that the $[Zn^{2+}(L^{\bullet-})(L'^{0})]$ description is the correct structure, although this will need further confirmation. Nevertheless, this work clearly demonstrates the importance of carefully selecting the level of computation to study the geometrical and electronic structures of this popular series of compounds and, by extension, all reduction processes for complexes including non-innocent ligands. In particular, the functionals with low amount of *exact* exchange ratio, as well as quite surprisingly, the CC2 method, should to be used with caution, even for optimizing geometries. The use of a method that does not provide correct geometry can have important consequences for the prediction of the molecular properties of these molecules in their reduced state. Further work is still needed to examine the role played by static correlation within these compounds in more detail, even for the closed-shell state.

Acknowledgments

M.K. thanks the Ecole polytechnique for a stipend. This research used resources of (i) local clusters; (ii) the Centre de Calcul Intensif des Pays de Loire (CCIPL); (iii) the Hopper cluster at the Phymath mésocentre, Ecole polytechnique/CNRS; (iv) HPC resources from GENCI-CINES/IDRIS (Grant A0020806894); and (v) HPC resources from ArronaxPlus (Grant No. ANR-11-EQPX-0004 funded by the French National Agency for Research).

Supporting Information

The supporting information is available free of charge on the ACS Publications website at DOI: XXX. Molecular orbitals, Spin density, Bond length variations, electronic energies and Cartesian coordinates.

Author information

Corresponding author

E-mail: gilles.frison@polytechnique.edu

ORCID

Duncan Carmichael : 0000-0002-9698-8943

Denis Jacquemin : 0000-0002-4217-0708

Gilles Frison : 0000-0002-5677-3569

Notes

The authors declare no competing financial interest.

References

(1) Schubert, U.S.; Eschbaumer, C. Macromolecules Containing Bipyridine and Terpyridine Metal Complexes: Towards Metallosupramolecular Polymers. *Angew. Chem. Int. Ed.* **2002**, *41*, 2892–2926.

(2) Peloquin, D.M.; Schmedake, T.A. Recent advances in hexacoordinate silicon with pyridine-containing ligands: Chemistry and emerging applications. *Coord. Chem. Rev.* **2016**, *323*, 107–119.

(3) Gray, P.A.; Krause, K.D.; Burford, N.; Patrick, B.O. Cationic 2,2'-bipyridine complexes of germanium(II) and tin(II). *Dalton Trans.* **2017**, *46*, 8363–8366.

(4) Barbieri, A.; Accorsi, G.; Armaroli, N. Luminescent complexes beyond the platinum group: the d^{10} avenue. *Chem. Commun.* **2008**, 2185–2193.

(5) Costa, R.D.; Orti, E.; Bolink, H.J.; Monti, F.; Accorsi, G.; Armaroli, N. Luminescent Ionic Transition-Metal Complexes for Light-Emitting Electrochemical Cells. *Angew. Chem. Int. Ed.* **2012**, *51*, 8178–8211.

(6) Le Bozec, H.; Guerchais, V. Photochromic bipyridyl metal complexes: Photoregulation of the nonlinear optical and/or luminescent properties. *C. R. Chimie* **2013**, *16*, 1172–1182.

(7) Andreiadis, E.S.; Chavarot-Kerlidou, M.; Fontecave, M.; Artero, V. Artificial Photosynthesis: From Molecular Catalysts for Light-driven Water Splitting to Photoelectrochemical Cells. *Photochem. Photobiol.* **2011**, *87*, 946–964.

(8) Kärkäs, M.D.; Verho, O.; Johnston, E.V.; Akermark, B. Artificial Photosynthesis: Molecular Systems for Catalytic Water Oxidation. *Chem. Rev.* **2014**, *114*, 11863–12001.

(9) Yoon, T.P.; Ischay, M.A.; Du, J. Visible light photocatalysis as a greener approach to photochemical synthesis. *Nat. Chem.* **2010**, *2*, 527–532.

(10) Prier, C.K.; Rankic, D.A.; MacMillan, D.W.C. Visible Light Photoredox Catalysis with Transition Metal Complexes: Applications in Organic Synthesis. *Chem. Rev.* **2013**, *113*, 5322–5363.

(11) Kalyanasundaram, K. PHOTOPHYSICS, PHOTOCHEMISTRY AND SOLAR ENERGY CONVERSION WITH TRIS(BIPYRIDYL)RUTHENIUM(II) AND ITS ANALOGUES. *Coord. Chem. Rev.* **1982**, *46*, 159–244.

(12) (a) Constable, E.C. Homoleptic complexes of 2,2'-bipyridine. *Adv. Inorg. Chem.* **1989**, *34*, 1–63; (b) Vlcek Jr., A.; Zalis, S. Modeling of charge-transfer transitions and excited states in d^6 transition metal complexes by DFT techniques. *Coord. Chem. Rev.* **2007**, *251*, 258–287.

(13) (a) Baryshnikov, G.V.; Minaev, B.F.; Korop, A.A., Minaeva, V.A.; Gusev, A.N. Structure of zinc complexes with 3-(pyridine-2-yl)-5-arylideneiminophenyl)-1H-1,2,4-triazoles in different tautomeric forms: DFT and QTAIM study. *Russ. J. Inorg. Chem.* **2013**, *58*, 928-934; (b) Gusev, A.N.; Shul'gin V.F.; Braga, E.V.; Nemec, I.; Minaev, B.F.; Baryshnikov, G.V.; Travnicek, Z.; Agren, H.; Eremenko, I.L.; Lyssenko, K.A.; Linert. W. Synthesis and photophysical properties of Zn(II) shiff base complexes possessing strong solvent-dependent solid-state fluorescence. *Polyhedron* **2018**, *155*, 202-208.

(14) Kaim, W. Manifestations of Noninnocent Ligand Behavior. *Inorg. Chem.* **2011**, *50*, 9752–9765.

(15) Turro, C.; Chung, Y.C.; Leventis, N.; Kuchenmeister, M.E.; Wagner, P.J.; Leroi, G.E. Resonance Raman Spectrum of the Phenanthroline Anion: Implications on Electron Delocalization in the MLCT Excited State of $Ru(phen)_3^{2+}$. *Inorg. Chem.* **1996**, *35*, 5104–5106.

(16) Pyo, S.; Perez-Cordero, E.; Bott, S.G.; Echegoyen, L. Crystal Structure of $[Ru(terpy)_2]^0$: A New Crystalline Material from the Reductive Electrocrystallization of $[Ru(terpy)_2]^{2+}$. *Inorg. Chem.* **1999**, *38*, 3337–3343.

(17) England, J.; Scarborough, C.C.; Weyhermüller, T.; Sproules, S.; Wieghardt, K. Electronic Structures of the Electron Transfer Series $[M(bpy)_3]^n$, $[M(tpy)_2]^n$, and $[Fe(^tbpy)_3]^n$ (M = Fe, Ru; *n* = 3+, 2+, 1+, 0, 1–): A Mössbauer Spectroscopic and DFT Study. *Eur. J. Inorg. Chem.* **2012**, 4605–4621.

(18) Bowman, A.C.; Sproules, S.; Wieghardt, K. Electronic Structures of the $[V(^tbpy)_3]^z$ (z = 3+, 2+, 0, 1−) Electron Transfer Series. *Inorg. Chem.* **2012**, *51*, 3707–3717.

(19) Bowman, A.C.; England, J.; Sproules, S.; Weyhermüller, T.; Wieghardt, K. Electronic Structures of Homoleptic $[Tris(2,2'\text{-bipyridine})M]^n$ Complexes of the Early Transition Metals (M = Sc, Y, Ti, Zr, Hf, V, Nb, Ta; n = 1+, 0, 1−, 2−, 3−): An Experimental and Density Functional Theoretical Study. *Inorg. Chem.* **2013**, *52*, 2242–2256.

(20) Wolff, C.; Gottschlich, A.; England, J.; Wieghardt, K.; Saak, W.; Haase, D.; Beckhaus, R. Molecular and Electronic Structures of Mononuclear and Dinuclear Titanium Complexes Containing π-Radical Anions of 2,2′-Bipyridine and 1,10-Phenanthroline: An Experimental and DFT Computational Study. *Inorg. Chem.* **2015**, *54*, 4811–4820.

(21) England, J.; Bill, E.; Weyhermüller, T.; Neese, F.; Atanasov, M.; Wieghardt, K. Molecular and Electronic Structures of Homoleptic Six-Coordinate Cobalt(I) Complexes of 2,2′:6′,2″-Terpyridine, 2,2′-Bipyridine, and 1,10-Phenanthroline. An Experimental and Computational Study. *Inorg. Chem.* **2015**, *54*, 12002–12018.

(22) Shit, M.; Maity, S.; Bera, S.; Weyhermüller, T.; Ghosh, P. Coordination of *o*-benzosemiquinonate, *o*-iminobenzosemiquinonate, 4,4'-di-*tert*-butyl-2,2'-bipyridine and 1,10-phenanthroline anion radicals to oxidovanadium(IV). *New J. Chem.* **2016**, *40*, 10305–10315.

(23) Duchackova, L.; Steinmetz, V.; Lemaire, J.; Roithova, J. Comparison of 2,2'-Bipyridine and 2,2'-Bipyridyl-N,N'-dioxide as Ligands in Zinc Complexes. *Inorg. Chem.* **2010**, *49*, 8897–8903.

(24) Kirketerp, M.B.S.; Brondsted Nielsen, S. Absorption spectrum of isolated tris(2,2'-bipyridine)ruthenium(II) dications *in vacuo. Int. J. Mass Spectrom*. **2010**, *297*, 63–66.

(25) Stockett, M.H.; Brondsted Nielsen, S. Does a single CH_3CN molecule attached to $Ru(bipy)_3^{2+}$ affect its absorption spectrum? *J. Chem. Phys.* **2015**, *142*, 171102.

(26) Skinnerup Byskov, C.; Weber, J.M.; Brondsted Nielsen, S. Gas-phase spectroscopy of singly reduced tris(bipyridine)ruthenium ions, $Ru(bipy)_3^+$. *Phys. Chem. Chem. Phys.* **2015**, *17*, 5561–5564.

(27) Katari, M.; Payen de la Garanderie, E.; Nicol, E.; Steinmetz, V.; van der Rest, G.; Carmichael, D.; Frison, G. Combining gas phase electron capture and IRMPD action spectroscopy to probe the electronic structure of a metastable reduced organometallic complex containing a non-innocent ligand. *Phys. Chem. Chem. Phys.* **2015**, *17*, 25689–25692.

(28) Xu, S.; Weber, J.M. Absorption Spectrum of a Ru(II)-Aquo Complex in Vacuo: Resolving Individual Charge-Transfer Transitions. *J. Phys. Chem. A* **2015**, *119*, 11509–11513.

(29) Xu, S.; Smith, J.E.T.; Weber, J.M. The electronic spectrum of cryogenic ruthenium-tris-bipyridine dications *in vacuo. J. Chem. Phys.* **2016***, 145*, 024304.

(30) Xu, S.; Smith, J.E.T.; Weber, J.M. UV Spectra of Tris(2,2'-bipyridine)−M(II) Complex Ions in Vacuo (M = Mn, Fe, Co, Ni, Cu, Zn). *Inorg. Chem.* **2016***, 55*, 11937-11943.

(31) Xu, S.; Smith, J.E.T.; Gozem, S.; Krylov, A.I.; Weber, J.M. Electronic Spectra of Tris(2,2'-bipyridine)-M(II) Complex Ions in Vacuo (M = Fe and Os). *Inorg. Chem.* **2017***, 56*, 7029-7037.

(32) Rannulu, N.S.; Rodgers, M.T. Noncovalent Interactions of Cu^+ with *N*-Donor Ligands (Pyridine, 4,4-Dipyridyl, 2,2-Dipyridyl, and 1,10-Phenanthroline): Collision-Induced Dissociation and Theoretical Studies. *J. Phys. Chem. A* **2012**, *116*, 1319–1332.

(33) Echegoyen, L.; DeCian, A.; Fischer, J.; Lehn, J.M. Cryptatium: A Species of Expanded Atom/Radical Ion Pair Type from Electroreductive Crystallization of the Macrobicyclic Sodium Tris(Bipyridine) Cryptate. *Angew. Chem. Int. Ed. Engl.* **1991**, *30*, 838–840.

(34) Chisholm, M.H.; Huffman, J.C.; Rothwell, I.P.; Bradley, P.G.; Kress, N.; Woodruff, W.H. Bis(2,2'-bipyridyl)diisopropoxymolybdenum(II). Structural and Spectroscopic Evidence for Molybdenum-to-Bipyridyl π^* Bonding. *J. Am. Chem. Soc.* **1981**, *103*, 4945–4947.

(35) Gore-Randall, E.; Irwin, M.; Denning, M.S.; Goicoechea, J.M. Synthesis and Characterization of Alkali-Metal Salts of 2,2'- and 2,4'-Bipyridyl Radicals and Dianions. *Inorg. Chem.* **2009**, *48*, 8304–8316.

(36) Bock, H.; Lehn, J.M.; Pauls, J.; Holl, S.; Krenzel, V. Sodium Salts of the Bipyridine Dianion: Polymer $[(bpy)^{2-}\{Na^+(dme)\}_2]_\infty$, Cluster $[(Na_8O)^{6+}Na^+_6\,(bpy)^{2-}_6\,(tmeda)_6]$, and Monomer $[(bpy)^{2-}\{Na^+(pmdta)\}_2]$. *Angew. Chem. Int. Ed.* **1999**, *38*, 952–955.

(37) Scarborough, C.C.; Sproules, S.; Weyhermüller, T.; DeBeer, S.; Wieghardt, K. Electronic and Molecular Structures of the Members of the Electron Transfer Series $[Cr(^tbpy)_3]^n$ (n = 3+, 2+, 1+, 0): An X-ray Absorption Spectroscopic and Density Functional Theoretical Study. *Inorg. Chem.* **2011**, *50*, 12446–12462.

(38) Wang, M.; Weyhermüller, T.; Bill, E.; Ye, S.; Wieghardt, K. Structural and Spectroscopic Characterization of Rhenium Complexes Containing Neutral, Monoanionic, and Dianionic Ligands of

2,2′-Bipyridines and 2,2′:6,2″-Terpyridines: An Experimental and Density Functional Theory (DFT)-Computational Study. *Inorg. Chem.* **2016**, *55*, 5019–5036.

(39) Wang, M.; Weyhermüller, T.; England, J.; Wieghardt, K. Molecular and Electronic Structures of Six-Coordinate "Low-Valent"$[M(^{Me}bpy)_3]^0$ (M = Ti, V, Cr, Mo) and $[M(tpy)_2]^0$ (M = Ti, V, Cr), and Seven-Coordinate $[MoF(^{Me}bpy)_3](PF_6)$ and $[MX(tpy)_2](PF_6)$ (M = Mo, X = Cl and M = W, X = F). *Inorg. Chem*. **2013**, *52*, 12763–12776.

(40) Wang, M.; Weyhermüller, T.; Wieghardt, K. Determining the Electronic Structure of a Series of $[(phen)_3M]^0$ (M = Ti, V, Mo) and $[(pdi)_2M]^{n+}$ (M = Cr, Mo) Complexes: Coordination of Neutral Ligands vs. π-Radical Anions. *Eur. J. Inorg. Chem.* **2015**, 3246–3254.

(41) (a) Scarborough, C.C.; Lancaster, K.M.; DeBeer, S.; Weyhermüller, T.; Sproules, S.; Wieghardt, K. Experimental Fingerprints for Redox-Active Terpyridine in $[Cr(tpy)_2]$ $(PF_6)_n$ (n = 3−0), and the Remarkable Electronic Structure of $[Cr(tpy)_2]^{1-}$. *Inorg. Chem.* **2012**, *51*, 3718–3732; (b) Wang, M.; England, J.; Weyhermüller, T.; Wieghardt, K. Molecular and Electronic Structures of the Members of the Electron Transfer Series $[Mn(bpy)_3]^n$ (n = 2+, 1+, 0, 1−) and $[Mn(tpy)_2]^m$ (m = 4+, 3+, 2+, 1+, 0). An Experimental and Density Functional Theory Study. *Inorg. Chem.* **2014**, *53*, 2276–2287.

(42) Skara, G.; Gimferrer, M.; De Proft, F.; Salvador, P. ; Pinter, B. Scrutinizing the noninnocence of quinone ligands in ruthenium complexes: insights from structural, electronic, energy, and effective oxidation state analyses. *Inorg. Chem.* **2016**, *55*, 2185-2199.

(43) Irwin, M.; Jenkins, R.K.; Denning, M.S.; Krämer, T.; Grandjean, F.; Long, G.J.; Herchel, R.; McGrady, J.E.; Goicoechea, J.M. Experimental and Computational Study of the Structural and Electronic Properties of Fe^{II}(2,2′-bipyridine)$(mes)_2$ and $[Fe^{II}$(2,2′-bipyridine)$(mes)_2]^-$, a Complex Containing a 2,2′-Bipyridyl Radical Anion. *Inorg. Chem.* **2010**, *49*, 6160–6171

(44) Irwin, M.; Doyle, L.R.; Krämer, T.; Herchel, R.; McGrady, J.E.; Goicoechea, J.M. A Homologous Series of First-Row Transition-Metal Complexes of 2,2′-Bipyridine and their Ligand Radical Derivatives: Trends in Structure, Magnetism, and Bonding. *Inorg. Chem.* **2012**, *51*, 12301–12312

(45) Wang, M.; England, J.; Weyhermüller, T.; Wieghardt, K. Electronic Structures of "Low-Valent" Neutral Complexes $[NiL_2]^0$ (*S* = 0; L = bpy, phen, tpy) – An Experimental and DFT Computational Study. *Eur. J. Inorg. Chem.* **2015**, 1511–1523.

(46) Wang, M.; Weyhermüller, T.; Wieghardt, K. The Electron Transfer Series $[Mo^{III}(bpy)_3]^n$ (n=3+, 2+, 1+, 0, 1–), and the Dinuclear Species $[\{Mo^{III}Cl(^{Me}bpy)_2\}_2(\mu_2\text{-}O)]Cl_2$ and $[\{Mo^{IV}(tpy^{\bullet})_2\}_2(\mu_2\text{-}MoO_4)](PF_6)_2\cdot 4MeCN$. *Chem. Eur. J.* **2014**, *20*, 9037–9044.

(47) Ma, X.; Suturina, E.A.; De, S.; Négrier, P.; Rouzières, M.; Clérac, R.; Dechambenoit, P. A Redox-Active Bridging Ligand to Promote Spin Delocalization, High-Spin Complexes, and Magnetic Multi-Switchability. *Angew. Chem. Int. Ed.* **2018**, *57*, 7841–7845.

(48) Sieh, D.; Schlimm, M.; Andernach, L.; Angersbach, F.; Nückel, S.; Schöffel, J.; Susnjar, N.; Burger, P. Metal–Ligand Electron Transfer in 4d and 5d Group 9 Transition Metal Complexes with Pyridine, Diimine Ligands. *Eur. J. Inorg. Chem.* **2012**, 444–462.

(49) Sieh, D.; Kubiak, C.P. A Series of Diamagnetic Pyridine Monoimine Rhenium Complexes with Different Degrees of Metal-to-Ligand Charge Transfer: Correlating ^{13}C NMR Chemical Shifts with Bond Lengths in Redox-Active Ligands. *Chem. Eur. J.* **2016**, *22*, 10638–10650.

(50) Scarborough, C.C.; Wieghardt, K. Electronic Structure of 2,2′-Bipyridine Organotransition-Metal Complexes. Establishing the Ligand Oxidation Level by Density Functional Theoretical Calculations. *Inorg. Chem.* **2011**, *50*, 9773–9793.

(51) Knijnenburg, Q.; Hetterscheid, D.; Kooistra, T.M.; Budzelaar, P.H.M. The Electronic Structure of (Diiminopyridine)cobalt(I) Complexes. *Eur. J. Inorg. Chem.* **2004**, 1204–1211.

(52) Budzelaar, P.H.M.; de Bruin, B.; Gal, A. W.; Wieghardt, K.; van Lenthe, J. H. Metal-to-Ligand Electron Transfer in Diiminopyridine Complexes of Mn-Zn. A Theoretical Study. *Inorg. Chem.* **2001**, *40*, 4649–4655.

(53) Ghosh, S.; Rahaman, A.; Holt, K.B.; Nordlander, E.; Richmond, M.G.; Kabir, S.E.; Hogarth, G. Hydrogenase biomimetics with redox-active ligands: Electrocatalytic proton reduction by $[Fe_2(CO)_4(\kappa^2$-diamine)(μ-edt)] (diamine = 2,2'-bipy, 1,10-phen). *Polyhedron* **2016**, *116*, 127–135

(54) Kalläne, S.I.; van Gastel, M. Raman Spectroscopy as a Method to Investigate Catalytic Intermediates: CO_2 Reducing $[Re(Cl)(bpy\text{-}R)(CO)_3]$ Catalyst. *J. Phys. Chem. A*, **2016**, *120*, 7465–7474.

(55) Cohen, A.J.; Mori-Sanchez, P.; Yang, W. Insights into current limitations of density functional theory. *Science* **2008**, *321*, 792–794.

(56) Peach, M.J.G.; Tozer, D.J. Overcoming Low Orbital Overlap and Triplet Instability Problems in TDDFT. *J. Phys. Chem. A* **2012**, *116*, 9783–9789.

(57) Laurent, A.D.; Jacquemin, D. TD-DFT Benchmarks: A Review. *Int. J. Quantum Chem.* **2013**, *113*, 2019–2039.

(58) Mewes, S.A.; Plasser, F.; Dreuw, A. Exciton analysis in time-dependent density functional theory: How functionals shape excited-state characters. *J. Chem. Phys.* **2015**, *143*, 171101.

(59) Gilson, A.I.; van der Rest, G.; Chamot-Rooke, J.; Kurlancheek, W.; Head-Gordon, M.; Jacquemin, D.; Frison, G. Ground Electronic State of Peptide Cation Radicals: A Delocalized Unpaired Electron? *J. Phys. Chem. Lett.* **2011**, *2*, 1426–1431.

(60) (a) Riffet, V.; Jacquemin, D.; Cauët, E.; Frison, G. Benchmarking DFT and TD-DFT Functionals for the Ground and Excited States of Hydrogen-Rich Peptide Radicals. *J. Chem. Theory Comput.* **2014**, *10*, 3308-3318; (b) Riffet, V.; Jacquemin, D.; Frison, G. H-atom loss and migration in hydrogen-rich peptide cation radicals: The role of chemical environment. *Int. J. Mass Spectrom.* **2015**, *390*, 28–38.

(61) Ashley, D.C.; Baik, M.H. The Electronic Structure of [Mn(V)=O]: What is the Connection between Oxyl Radical Character, Physical Oxidation State, and Reactivity? *ACS Catal.* **2016**, *6*, 7202–7216.

(62) (a) Conradie, J.; Ghosh, A. DFT Calculations on the Spin-Crossover Complex Fe(salen)(NO): A Quest for the Best Functional. *J. Phys. Chem. B* **2007**, *111*, 12621–12624; (b) Boguslawski, K.; Jacob, C.R.; Reiher, M. Can DFT Accurately Predict Spin Densities? Analysis of Discrepancies in Iron Nitrosyl Complexes. *J. Chem. Theory Comput.* **2011**, *7*, 2740–2752.

(63) Baryshnikov, G.V.; Minaev, B.F.; Slepets, A.A.; Minaeva, V.A. A study of the role played by the Hartree-Fock orbital exchange in the formation of the energy of the first singlet charge-transfer excited state by the example of JK-62 and JK-201 sensitizing dye molecules. *Opt. Spectrosc.* **2014**, *116*, 431-437.

(64) Ioannidis, E.I.; Kulik, H.J. Ligand-field-dependent behavior of meta-GGA exchange in transition-metal complex spin-state ordering. *J. Phys. Chem. A* **2017**, *121*, 874-884.

(65) Minaev, B.; Baryshnikova, A.; Sun, W.H. Spin-dependent effects in ethylene polymerization with bis(imino)pyridine iron(II) complexes. *J. Organomet. Chem.* **2016**, *811*, 48-65.

(66) (a) Scarborough, C.C.; Sproules, S.; Doonan, C.J.; Hagen, K.S.; Weyhermüller, T.; Wieghardt, K. Scrutinizing Low-Spin Cr(II) Complexes. *Inorg. Chem.* **2012**, *51*, 6969–6982; (b) Chan, S.C.; England, J.; Lee, W.C.; Wieghardt, K.; Wong, C.Y. Noninnocent Behavior of Nitrosoarene–Pyridine Hybrid Ligands: Ruthenium Complexes Bearing a 2-(2-Nitrosoaryl)Pyridine Monoanion Radical. *ChemPlusChem*, **2013**, *78*, 214–217.

(67) Wang, M.; England, J.; Weyhermüller, T.; Kokatam, S.L.; Pollock, C.J.; DeBeer, S.; Shen, J.; Yap, G.P.A.; Theopold, K.H.; Wieghardt, K. New Complexes of Chromium(III) Containing Organic π-Radical Ligands: An Experimental and Density Functional Theory Study. *Inorg. Chem.* **2013**, *52*, 4472–4487.

(68) Bezdek, M.J.; Guo, S.; Chirik, P.J. Terpyridine Molybdenum Dinitrogen Chemistry: Synthesis of Dinitrogen Complexes That Vary by Five Oxidation States. *Inorg. Chem.* **2016**, *55*, 3117–3127.

(69) Sinha, S.; Das, S.; Sikari, R.; Parua, S.; Brandao, P.; Demeshko, S.; Meyer, F.; Paul, N.D. Redox Noninnocent Azo-Aromatic Pincers and Their Iron Complexes. Isolation, Characterization, and Catalytic Alcohol Oxidation. *Inorg. Chem.* **2017**, *56*, 14084–14100.

(70) Rath, S.P.; Sengupta, D.; Ghosh, P.; Bhattacharjee, R.; Chakraborty, M.; Samanta, S.; Datta, A.; Goswami, S. Effects of Ancillary Ligands on Redox and Chemical Properties of Ruthenium Coordinated Azoaromatic Pincer. *Inorg. Chem.* **2018**, *57*, 11995-12009.

(71) (a) Gowda, A.S.; Petersen, J.L.; Milsmann, C. Redox Chemistry of Bis(pyrrolyl)pyridine Chromium and Molybdenum Complexes: An Experimental and Density Functional Theoretical Study. *Inorg. Chem.* **2018**, *57*, 1919–1934; (b) Lefebvre, J.F.; Schindler, J.; Traber, P.; Zhang, Y.; Kupfer, S.; Gräfe, S.; Baussanne, I.; Demeunynck, M.; Mouesca, J.M.; Gambarelli, S.; Artero, V.; Dietzek, B.; Chavarot-Kerlidou, M. An artificial photosynthetic system for photoaccumulation of two electrons on a fused dipyridophenazine (dppz)–pyridoquinolinone ligand. *Chem. Sci.* **2018**, *9*, 4152–4159; (c) Lin, Z.; Thacker, N.C.; Sawano, T.; Drake, T.; Ji, P.; Lan, G.; Cao, L.; Liu, S.; Wang, C.; Lin, W. Metal–organic layers stabilize earth-abundant metal–terpyridine diradical complexes for catalytic C–H activation. *Chem. Sci.* **2018**, *9*, 143–151.

(72) (a) Pierloot, K.; Vancoillie, S. Relative energy of the high-($^5T_{2g}$) and low-($^1A_{1g}$) spin states of $[Fe(H_2O)_6]^{2+}$, $[Fe(NH_3)_6]^{2+}$, and $[Fe(bpy)_3]^{2+}$: CASPT2 versus density functional theory. *J. Chem. Phys.* **2006**, *125*, 124303; (b) Milko, P.; Iron, M.A. On the innocence of bipyridine ligands: how well do DFT functionals fare for these challenging spin systems? *J. Chem. Theory Comput.* **2014**, *10*, 220-235; (c) Zell, T.; Milko, P.; Fillman, K.L.; Diskin-Posner, Y.; Bendikov, T.; Iron, M.A.; Leitus, G.; Ben-David, Y.; Neidig, M.L.; Milstein, D. Iron dicarbonyl complexes featuring bipyridine-based PNN pincer ligands with short interpyridine C-C bond lengths: innocent or non-innocent ligand? *Chem. Eur. J.* **2014**, *20*, 4403-4413; (d) Ortuno, M.A.; Cramer, C.J.; Multireference electronic structures of Fe-pyridine(diamine) complexes over multiple oxidation states. *J. Phys. Chem. A* **2017**, *121*, 5932-5939.

(73) Stroh, C.; Belorizky, E.; Turek, P.; Bolvin, H.; Ziessel, R. Aminomethyl-bipyridine bearing two flexible nitronyl-nitroxide arms: a new podand for complexation of transition metals in a facial or meridional conformation. *Inorg. Chem.* **2003**, *42*, 2938-2949.(74) Boricha, V.P.; Patra, S.; Chouhan, Y.S.; Sanavada, P.; Suresh, E.; Paul, P. Synthesis, Characterisation, Electrochemistry and Ion-Binding Studies of Ruthenium(II) and Rhenium(I) Bipyridine/Crown Ether Receptor Molecules. *Eur. J. Inorg. Chem.* **2009**, 1256–1267.

(75) McDaniel, A.M.; Tseng, H.W.; Damrauer, N.H.; Shores, M.P. Synthesis and Solution Phase Characterization of Strongly Photooxidizing Heteroleptic Cr(III) Tris-Dipyridyl Complexes. *Inorg. Chem.* **2010**, *49*, 7981–7991.

(76) Katari, M.; Nicol, E.; Steinmetz, V.; van der Rest, G.; Carmichael, D.; Frison, G. Improved Infrared Spectra Prediction by DFT from a New Experimental Database. *Chem. Eur. J.* **2017**, 23, 8414–8423.

(77) Fontanesi, C.; Benassi, R.; Giovanardi, R.; Marcaccio, M.; Paolucci, F.; Roffia, S. Computational electrochemistry. Ab initio calculation of solvent effect in the multiple electroreduction of polypyridinic compounds. *J. Mol. Struct.* **2002**, *612*, 277–286.

(78) Chiang, L.; Herasymchuk, K.; Thomas, F.; Storr, T. Influence of Electron-Withdrawing Substituents on the Electronic Structure of Oxidized Ni and Cu Salen Complexes. *Inorg. Chem.* **2015**, *54*, 5970ï 5980.

(79) Frisch, M.J.; Trucks, G.W.; Schlegel, H.B.; Scuseria, G.E.; Robb, M.A.; Cheeseman, J.R.; Scalmani, G.; Barone, V.; Mennucci, B.; Petersson, G.A.; Nakatsuji, H.; Caricato, M.; Li, X.; Hratchian, H.P.; Izmaylov, A.F.; Bloino, J.; Zheng, G.; Sonnenberg, J.L.; Hada, M.; Ehara, M.; Toyota, K.; Fukuda, R.; Hasegawa, J.; Ishida, M.; Nakajima, T.; Honda, Y.; Kitao, O.; Nakai, H.; Vreven, T.; Montgomery, J.A.

Jr.; Peralta, J.E.; Ogliaro, F.; Bearpark, M.; Heyd, J.J.; Brothers, E.; Kudin, K.N.; Staroverov, V.N.; Keith, T.; Kobayashi, R.; Normand, J.; Raghavachari, K.; Rendell, A.; Burant, J.C.; Iyengar, S.S.; Tomasi, J.; Cossi, M.; Rega, N.; Millam, J.M.; Klene, M.; Knox, J.E.; Cross, J.B.; Bakken, V.; Adamo, C.; Jaramillo, J.; Gomperts, R.; Stratmann, R.E.; Yazyev, O.; Austin, A.J.; Cammi, R.; Pomelli, C.; Ochterski, J.W.; Martin, R.L.; Morokuma, K.; Zakrzewski, V.G.; Voth, G.A.; Salvador, P.; Dannenberg, J.J.; Dapprich, S.; Daniels, A.D.; Farkas, Ö.; Foresman, J.B.; Ortiz, J.V.; Cioslowski, J.; Fox, D.J. Gaussian, Inc., Wallingford CT, **2013**, Gaussian 09 (Revision D.01).

(80) Becke, A.D. Density-functional exchange-energy approximation with correct asymptotic behavior. *Phys. Rev. A*, **1988**, *38*, 3098ï 3100.

(81) (a) Lee, C.; Yang, W.; Parr, R.G. Development of the Colle-Salvetti correlation-energy formula into a functional of the electron density. *Phys. Rev. B* **1988**, *37*, 785–789; (b) Becke, A.D. Density-functional thermochemistry. III. The role of exact exchange. *J. Chem. Phys*. **1993**, *98*, 5648–5652.

(82) Yanai, T.; Tew, D.; Handy, N. A new hybrid exchange–correlation functional using the Coulomb-attenuating method (CAM-B3LYP). *Chem. Phys. Lett.* **2004**, *393*, 51–57.

(83) Iikura, H.; Tsuneda, T.; Yanai, T.; Hirao, K. A long-range correction scheme for generalized-gradient-approximation exchange functionals. *J. Chem. Phys.* **2001**, *115*, 3540–3544.

(84) Zhao, Y.; Truhlar, D.G. A new local density functional for main-group thermochemistry, transition metal bonding, thermochemical kinetics, and noncovalent interactions. *J. Chem. Phys.* **2006**, *125*, 194101.

(85) Zhao, Y.; Truhlar, D.G. The M06 suite of density functionals for main group thermochemistry, thermochemical kinetics, noncovalent interactions, excited states, and transition elements: two new functionals and systematic testing of four M06-class functionals and 12 other functionals. *Theor. Chem. Acc.* **2008**, *120*, 215–241.

(86) Zhao, Y.; Truhlar, D.G. Comparative DFT study of van der Waals complexes: Rare-gas dimers, alkaline-earth dimers, zinc dimer, and zinc-rare-gas dimers. *J. Phys. Chem.* **2006**, *110*, 5121–5129.

(87) Chai, J.D.; Head-Gordon, M. Long-range corrected hybrid density functionals with damped atom-atom dispersion corrections. *Phys. Chem. Chem. Phys.* **2008**, *10*, 6615–6620.

(88) Chai, J.D.; Head-Gordon, M. Systematic optimization of long-range corrected hybrid density functionals. *J. Chem. Phys.* **2008**, *128*, 084106.

(89) Perdew, J.P.; Burke, K.; Ernzerhof, M. Generalized gradient approximation made simple. *Phys. Rev. Lett.* **1996**, *77*, 3865-3868.

(90) Adamo, C.; Barone, V. Toward reliable density functional methods without adjustable parameters: The PBE0 model. *J. Chem. Phys.* **1999**, 110, 6158-6169.

(91) Tao, J.M.; Perdew, J.P.; Staroverov, V.N.; Scuseria, G.E. Climbing the density functional ladder: Nonempirical meta-generalized gradient approximation designed for molecules and solids. *Phys. Rev. Lett.* **2003**, *91*, 146401.

(92) Staroverov, V.N.; Scuseria,G.E.; Tao, J.; Perdew, J.P. Comparative assessment of a new nonempirical density functional: Molecules and hydrogen-bonded complexes. *J. Chem. Phys.* **2003**, *119*, 12129.

(93) Peverati, R.; Truhlar, D.G. Improving the Accuracy of Hybrid Meta-GGA Density Functionals by Range Separation. *J. Phys. Chem. Lett.* **2011**, *2*, 2810-2817

(94) Weigend, F.; Ahlrichs, R. Balanced basis sets of split valence, triple zeta valence and quadruple zeta valence quality for H to Rn: Design and assessment of accuracy. *Phys. Chem. Chem. Phys.* **2005**, *7*, 3297–3305.

(95) Purvis, G.D.; Bartlett, R.J. A full coupled-cluster singles and doubles model: The inclusion of disconnected triples. *J. Chem. Phys.*, **1982**, *76*, 1910–1918.

(96) (a) Christiansen, O.; Koch, H.; Jørgensen, P. The second-order approximate coupled cluster singles and doubles model CC2. *Chem. Phys. Lett.*, **1995**, *243*, 409–418; (b) $\mathbf{3}^{\bullet-}$ could not be obtained at the CC2 level due to convergence problem.

(97) Frisch, M.J.; Trucks, G.W.; Schlegel, H.B.; Scuseria, G.E.; Robb, M.A.; Cheeseman, J.R.; Scalmani, G.; Barone, V.; Petersson, G.A.; Nakatsuji, H.; Caricato, M.; Marenich, A.V.; Bloino, J.; Janesko, B.G.; Gomperts, R.; Mennucci, B.; Hratchian, H.P.; Ortiz, J.V.; Izmaylov, A.F.; Sonnenberg, J.L.; Williams-Young, D.; Ding, F.; Lipparini, F.; Egidi, F.; Goings, J.; Peng, B.; Petrone, A.; Henderson, T.; Ranasinghe, D.; Zakrzewski, V.G.; Gao, J.; Rega, N.; Zheng, G.; Liang, W.; Hada, M.; Ehara, M.; Toyota, K.; Fukuda, R.; Hasegawa, J.; Ishida, M.; Nakajima, T.; Honda, Y.; Kitao, O.; Nakai, H.; Vreven, T.; Throssell, K.; Montgomery, J.A. Jr.; Peralta, J.E.; Ogliaro, F.; Bearpark, M.; Heyd, J.J.; Brothers, E.; Kudin, K.N.; Staroverov, V.N.; Keith, T.; Kobayashi, R.; Normand, J.; Raghavachari, K.; Rendell, A.; Burant, J.C.; Iyengar, S.S.; Tomasi, J.; Cossi, M.; Millam, J.M.; Klene, M.; Adamo, C.; Cammi, R.; Ochterski, J.W.; Martin, R.L.; Morokuma, K.; Farkas, Ö.; Foresman, J.B.; Fox, D.J. Gaussian, Inc., Wallingford CT, **2016**, Gaussian 16 (Revision B.01).

(98) TURBOMOLE V7.1 **2018**, a development of University of Karlsruhe and Forschungszentrum Karlsruhe GmbH, 1989-2007, TURBOMOLE GmbH, since 2007; available from http://www.turbomole.com.

(99) Parrish, R.M.; Burns, L.A.; Smith, D.G.A.; Simmonett, A.C.; DePrince III, A.E.; Hohenstein, E.G.; Bozkaya, U.; Sokolov, A.Yu.; Di Remigio, R.; Richard, R.M.; Gonthier, J.F.; James, A.M.; McAlexander, H.R.; Kumar, A.; Saitow, M.; Wang, X.; Pritchard, B.P.; Verma, P.; Schaefer III, H.F.; Patkowski, K.; King, R.A.; Valeev, E.F.; Evangelista, F.A.; Turney, J.M.; Crawford, T.D.; Sherrill, C.D. Psi4 1.1: An Open-Source Electronic Structure Program Emphasizing Automation, Advanced Libraries, and Interoperability. *J. Chem. Theory Comput.* **2017**, *13***,** 3185–3197.

(100) (a) Budzak, S.; Scalmani, G.; Jacquemin, D. Accurate Excited-State Geometries: A CASPT2 and Coupled-Cluster Reference Database for Small Molecules. *J. Chem. Theory Comput.* **2017**, *13*, 6237-6252; (b)Brémond, E.; Savarese, M.; Adamo, C.; Jacquemin, D. Accuracy of TD-DFT Geometries: A Fresh Look. *J. Chem. Theory Comput.* **2018**, *14*, 3715–3727.

(101) Helgaker, T.; Gauss, J.; Jorgensen, P.; Olsen, J. The prediction of molecular equilibrium structures by the standard electronic wave functions. *J. Chem. Phys.* **1997**, *106*, 6430–6440.

(102) $\mathbf{2a}^{\bullet-}$ could not be obtained at the CCSD(Full)/6-311G(d,p) level due to excessive memory requirement.

(103) (a) Reed, A.E.; Weinstock, R.B.; Weinhold, F. Natural population analysis. *J. Chem. Phys.* **1985**, *83*, 735–746; (b) Reed, A.E.; Weinhold, F. Natural localized molecular orbitals. *J. Chem. Phys.* **1985**, *83*, 1736–1740.

(104) Neese, F. Software update: the ORCA program system, version 4.0. *WIREs Comput. Mol. Sci.* **2018**, *8*, e1327.

(105) (a) Grimme, S.; Hansen, A. A practicable real-space measure and visualization of static electron-correlation effects. *Angew. Chem. Int. Ed.* **2015**, *54*, 12308-12313; (b) Bauer, C.A.; Hansen, A.; Grimme, S. The fractional occupation number weighted density as a versatile analysis tool for molecules with a complicated electronic structure. *Chem. Eur. J.* **2017**, *23*, 6150-6164.

(106) Witwicki, M.; Density functional theory and ab initio studies on hyperfine coupling constants of phosphinyl radicals. *Int. J. Quantum Chem.* **2018**, *118*, e25779; (b) In-Iam, A.; Wolf, M.; Wilfer, C.; Schaniel, D.; Woike, T.; Klüfers, P. $\{FeNO\}^7$-type halogenido nitrosyl ferrates: syntheses, bonding, and photoindiced linkage isomerism. *Chem. Eur. J.* **2019**, *25*, 1304-1325.

(107) Chung, G.; Lee, D. Molecular Structures of 2,2-Bipyridine and Its Anion Radical: Multiconfiguration-SCF Calculations . *Bull. Korean, Chem. Soc.* **2008**, *29*, 2419–2422.

(108) Artiukhin, D.G.; Stein, C.J.; Reiher, M.; Neugebauer, J. Quantum Chemical Spin Densities for Radical Cations of Photosynthetic Pigment Models. *Photochem. Photobiol.* **2017**, *93*, 815–833.

For Table of Contents Only

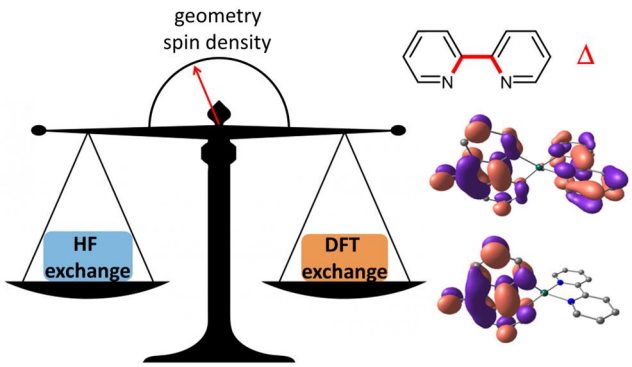

Bidentate N-heterocyclic ligands and their complexes are known to change their geometry upon electronic reduction, as a function of the localization of the added electron. The influence of the HF-like exchange on the accuracy of these parameters is evaluated by comparison with X-ray structures and coupled-cluster calculations.